INORGANIC CHEMISTRY

FRONTIERS

Accepted Manuscript

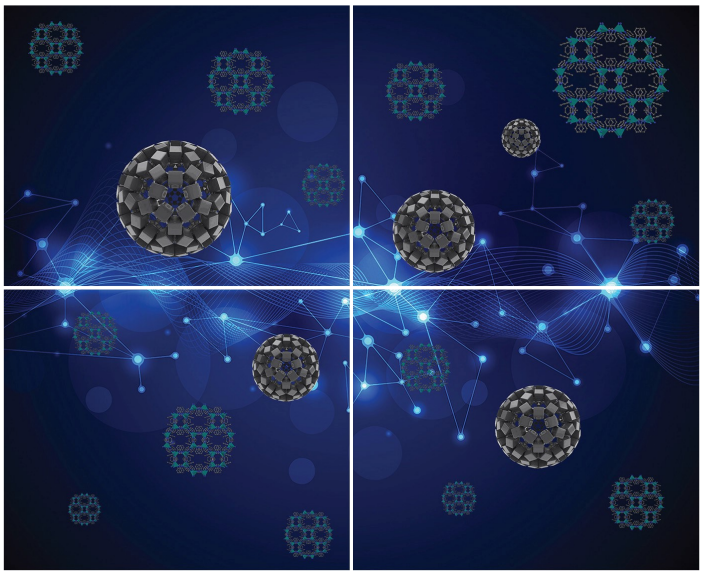

This article can be cited before page numbers have been issued, to do this please use: C. Fan, Q. Zhang, Y. Wang, Y. Jin and Q. He, *Inorg. Chem. Front.*, 2025, DOI: 10.1039/D5QI01376C.

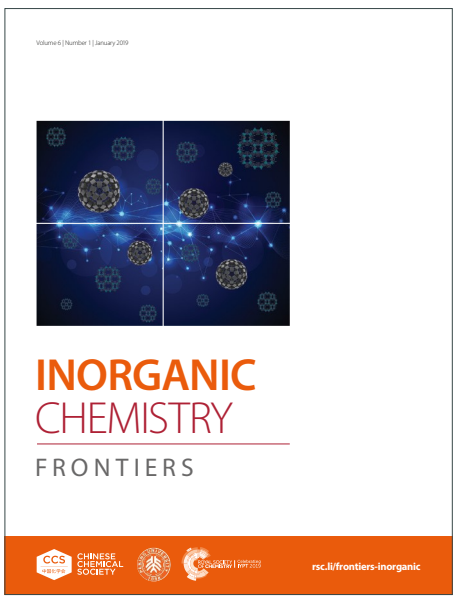

View Article Online
DOI: 10.1039/D5QI01376C

Constructing core-shell SiC@C nanofiber network structure to enhance conductive loss for efficient microwave absorption

Yingzhi Jin[1], Congmin Fan*[1], Qiaoling Zhang[1], Qinchuan He[1], Yiqun Wang*[1]

1. College of Materials and Chemistry & Chemical Engineering, Chengdu University of Technology, Chengdu, 610059, Sichuan, P.R.China

*Corresponding author: Yiqun Wang, and Congmin Fan

E-mail: wangyiqun17@cdut.edu.cn (Yiqun Wang)

fcongmin@mail.ustc.edu.cn (Congmin Fan)

Abstracts

The inherent impedance mismatch and limited electrical conductivity of SiC constrain its effectiveness as an electromagnetic wave absorber. However, rational microstructural design offers a viable strategy to enhance both impedance matching and conductive loss. In this study, core-shell structured SiC@C nanofibers were successfully fabricated via a coaxial electrospinning technique combined with a high-temperature carbothermal reduction process. The hollow core-shell structure was formed by controlling the carbon thermal reduction temperature to achieve the diffusion reaction between carbon and SiO_2, which synergistically improved the impedance matching of the composite with SiO_2. Additionally, excess carbon enhanced the conductive properties of the composite. The interconnected nanofiber structure created a comprehensive three-dimensional conductive network. This integrated network significantly enhanced the composite's conductive loss mechanisms, which consequently led to superior electromagnetic wave attenuation capabilities. The composite exhibited outstanding electromagnetic wave absorption performance at 1450 ℃, achieving a notable minimum reflection loss of -66.64 dB. Furthermore, at an optimal matching thickness of 2.09 mm, core-shell SiC@C nanofibers achieved a maximum effective absorption bandwidth of 7.52 GHz, covering the frequency range from 9.28 to 16.8 GHz. This work not only presents a strategy for designing core–shell

structured SiC@C nanofibers, but also offers new insights into impedance matching regulation and the construction of efficient conductive networks.

Keywords: Core-shell structure; Electromagnetic wave absorption; Conductive network; Impedance matching; Heterojunction;

1 Introduction

With the rapid advancement of information technology, electromagnetic interference has become an increasingly serious environmental concern. This rising form of pollution significantly impacts both industrial operations and daily life across the globe[1-4]. Simultaneously, the growing demands of military stealth applications continue to raise performance requirements for electromagnetic wave-absorbing materials. Consequently, the development of absorbers that combine strong reflection loss with broad effective absorption bandwidth is of great importance[5-9]. The contemporary exploration and innovation in highly effective microwave-absorbing materials (MAMs) encompasses diverse material categories. These include carbon-derived compositions[10], ferrous-based compounds[11], ceramic-structured substances[12-14], as well as electrically conductive polymeric materials[15]. SiC stands out as an exemplary dielectric ceramic, attracting significant attention from researchers due to its exceptional thermal stability, outstanding resistance to chemical and oxidative degradation, and excellent mechanical durability[16-18]. Wang and colleagues produced SiC powders through the pyrolysis of polycarbosilane, achieving a minimum reflection loss (RL_{min}) of -35 dB and an effective absorption bandwidth (EAB) measuring 1.34 GHz[19]. Utilizing an in-situ reactive growth methodology, Yan and collaborators fabricated SiC aerogels that demonstrated a RL_{min} of -40.7 dB at a thickness of 5.5 mm[20]. Through a combination of sol-gel processing, freeze-drying techniques, and the polymer-derived ceramics approach, Liu and associates developed SiC ceramic aerogels. These materials exhibited a RL_{min} of -26.5 dB at a frequency of 11.98 GHz when configured at the optimal thickness of 2.5 mm, while achieving an EAB of 5.4 GHz[21]. Although a lot of research has been carried out around SiC, its poor impedance matching as an electromagnetic wave (EMW) absorber still needs to be solved.

View Article Online
DOI: 10.1039/D5QI01376C

Microstructural characteristics play a pivotal role in determining the overall performance of MAMs. Through deliberate microstructural engineering, electromagnetic wave penetration can be significantly improved, thereby optimizing impedance matching and enhancing absorption efficiency. This strategy has become a central focus in current research on EMW absorbers. Recent scientific advances have led to the successful design of a wide range of structural architectures across multiple dimensional scales, including zero-dimensional structures[22], linear one-dimensional formations[23-25], planar two-dimensional arrangements[26], and comprehensive three-dimensional frameworks[27]. Among these, one-dimensional nanofiber structures demonstrate greater versatility and potential than zero-dimensional nanoparticles in tuning electromagnetic parameters, enhancing impedance matching, and facilitating multiple loss mechanisms[28]. Nanofiber materials offer advantages such as low density and high specific surface area, while their unique fiber morphology optimizes the propagation paths of EMWs within the material, enhancing wave–material interactions. Furthermore, nanofibers with high aspect ratios and interwoven structures can form a three-dimensional continuous conductive network, increasing electron transport pathways and significantly improving the material's electrical conductivity. Zhang and colleagues synthesized nitrogen-doped, bean-shaped SiC-based nanofibers structures utilizing a combination of electrospinning techniques and straightforward high-temperature pyrolytic processing. These engineered materials demonstrated exceptional electromagnetic properties when configured at an optimal thickness of 4 mm, achieving a RL_{min} of -51.8 dB at 6.3 GHz frequency, while maintaining an EAB of 2.8 GHz[29]. Zhang et al. achieved -38.2 dB RL_{min} and 4.5 GHz EAB with flexible SiC/TiC hybrid nanofibers prepared by electrostatic spinning and precursor infiltration pyrolysis[30]. Research has shown that fabricating core–shell architectures creates distinct heterogeneous interfaces, which enhance interfacial polarization effects and thereby improve the microwave attenuation performance of the materials[31]. Chen and associates employed a heat-facilitated surface adhesion methodology to fabricate core-shell structured SiC@Ni composites. These materials exhibited a RL_{min} of -22.45 dB at a frequency of 8.7 GHz, while maintaining an EAB spanning 2.5 GHz[32]. SiC/rGO

core-shell nanowires with -56.3 dB RL_{min} and 6.2 GHz EAB_{max} prepared by solution electrostatic spinning and annealing treatment by Wang et al[33]. All these indicate that reasonable nanofiber structure and core-shell structure design can achieve significant improvement in EMW absorption performance.

Beyond structural design, impedance matching can also be optimized through careful compositional tuning. SiC possesses exceptional chemical stability and high-temperature resistance. However, introducing different components often alters the overall performance of the absorbing material. The incorporation of magnetic transition elements such as Fe, Co, and Ni can enhance both magnetic and dielectric characteristics, thereby facilitating improved impedance matching. However, under high-temperature conditions, these metallic components oxidize, leading to the deterioration of their magnetic properties. This degradation results in a gradual decline in the electromagnetic wave attenuation performance of SiC-based composite systems. Therefore, retaining the original unique properties of SiC during the process of structural design and component introduction has become a research hotspot.

In this work, core-shell SiC@C nanofibers were successfully synthesized by combining coaxial electrospinning with high-temperature carbothermal reduction. By precisely controlling the reduction temperature, a diffusion reaction between carbon and SiO_2 was facilitated, resulting in the formation of a hollow core-shell structure. The results show that they exhibit different EMW absorption characteristics at different high temperature pyrolysis temperatures. Upon reaching a thermal threshold of 1450℃, the specimen demonstrates extraordinary electromagnetic properties: a minimum reflection loss of -66.64 dB at 6.48 GHz with a corresponding thickness of 3.60 mm, alongside a maximum effective absorption bandwidth of 7.52 GHz when configured at a thickness of 2.09 mm. The research presented herein contributes valuable methodological approaches for engineering specialized core-shell nanofibers architectures, while simultaneously offering significant insights that advance the development of superior electromagnetic wave absorption systems and radar-evading technological materials.

2 Experimental

View Article Online
DOI: 10.1039/D5QI01376C

2.1 Materials

The polymer polyacrylonitrile (PAN) with a molecular weight of 150000 g/mol was sourced from Sigma-Aldrich corporation. N,N-dimethylformamide (DMF, 99.5%) and polyvinylpyrrolidone (PVP, Mw = 1300000 g/mol) were supplied by Shanghai McLean Biochemical Technology Co. Polycarbosilane (PCS) was produced from Xiamen University. All reagents are unpurified.

2.2 Preparation of core-shell SiC@C nanofibers

Firstly, prepare two different solutions. PAN (1 g) underwent dissolution in DMF (10 mL) with continuous magnetic agitation for a duration of 3 hours, yielding a transparent mixture designated as Solution I. Concurrently, appropriate quantities of PCS and PVP were solubilized in a binary solvent system comprising chloroform (8 mL) and DMF (2 mL). This mixture was subjected to magnetic agitation for an equivalent 3-hour period, resulting in a homogeneous formulation labeled Solution II. Both prepared solutions were subsequently transferred into separate 10 mL syringes for the coaxial electrospinning process. The apparatus employed featured coaxial stainless steel needles with distinct shell and core compartments. Solution I was introduced into the shell chamber while Solution II occupied the core chamber. Operational parameters for the electrospinning procedure were established as follows: a shell-to-core feed rate ratio of 2:1, a needle-tip-to-collector distance of 15 cm, an applied voltage of 22 kV, and a collector drum rotational velocity of 200 revolutions per minute. After electrostatic spinning, the samples were dried in a vacuum oven at 70℃ for 24 h and pre-oxidation for 2 h in a blast oven at 240℃. Then the pyrolysis was carried out at 1400℃, 1450℃, 1500℃, 1550℃, and 1600℃ under N_2 atmosphere, named SCNF-1400, SCNF-1450, SCNF-1500, SCNF-1550, and SCNF-1600, respectively.

2.3 Characterization

Crystallographic analysis of the fabricated nanofibers composites was performed utilizing a SmartLab 9Kw X-ray diffraction system. Vibrational spectroscopic measurements were acquired with a HORIBA LabRAM hr800 Raman microscopic apparatus. Surface chemical composition analysis and elemental state determination

were conducted via ESCA PHI 5400 X-ray photoelectron spectroscopy instrumentation. Morphological examination, microstructural evaluation, and dimensional assessment of the core-shell SiC@C nanofibers architectures were accomplished through complementary microscopic techniques: Zeiss Sigma500 scanning electron microscopy and FEI Talos F200S transmission electron microscopy. Electromagnetic characterization was executed using an Agilent N5244A vector network analyzer operating in the 2-18 GHz frequency range. Paraffin wax was added to the sample at 10% by weight, and the resulting composite mixture was pressed into a coaxial annular mold to produce annular specimens with precisely controlled dimensions: thickness 2.00 mm, outer diameter 7.00 mm, and inner diameter 3.04 mm.

3 Results and discussion

3.1 Structure and morphology

View Article Online
DOI: 10.1039/D5QI01376C

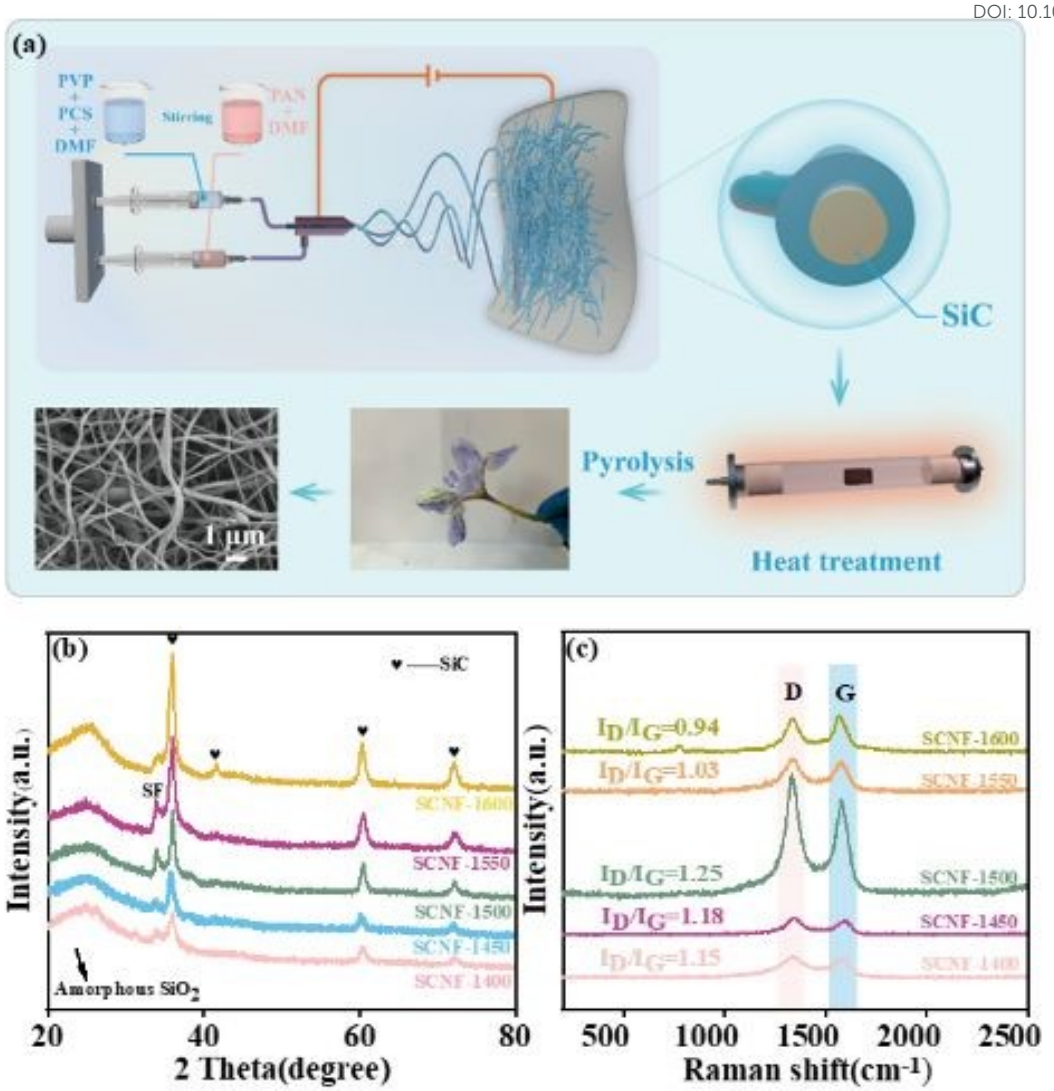

Fig. 1 (a) Schematic of the preparation of core-shell SiC@C nanofibers; (b) XRD patterns and (c) Raman spectra of SCNF-1400 to SCNF-1600

The synthetic methodology for fabricating core-shell SiC@C nanofibers composites is illustrated schematically in Fig. 1a. Firstly, PAN is used as a carbon source through coaxial electrospinning to make it inside, and PCS is used as a silicon source to coat the outside of the PAN fiber. Under high temperature environment, PAN is cracked to form carbon fiber, while the external PCS is cracked to obtain a SiO_2 shell. As the temperature rises, the internal C diffuses outward and reacts with SiO_2 to form a hollow SiC fiber.

The XRD patterns of SCNF-1400 to SCNF-1600 are shown in Fig. 1b. It can be observed that all samples have three diffraction peaks at 35.7°, 60.1° and 71.9° corresponding to the (111), (220) and (311) crystallographic alignments of β-SiC

(JCPDS#29-1129), respectively[26], which suggests that the prepared SCNF fibers contain the β-SiC phase. Concurrently, with the increase of carbothermal reduction temperature, the three β-SiC characteristic peaks gradually become sharper, which means that the crystallinity of β-SiC phase is enhanced. A broad and diffuse peak is present in the range of 15°-30°, corresponding to the characteristic amorphous band of SiO_2, which indicates that there is excess SiO_2 that has not reacted completely[34]. In addition, a weak diffraction peak, labelled "SF", can be observed at 33.7° in front of the diffraction peak of the (111) crystal plane, which is related to the stacking lamination of β-SiC[35]. The intensity of the "SF" peak increases and then decreases with the increase of temperature, and reaches the maximum value at 1550℃. This is due to the formation of defects due to incomplete crystallisation of β-SiC. When the temperature reaches 1600℃, β-SiC can be well rearranged to form complete crystals, so the diffraction peaks are weakened. Stacked layer defects disrupt the otherwise uniform charge distribution, creating additional trapping sites for charge carriers such as electrons and holes. Moreover, quantum confinement effects at the β-SiC interfacial boundaries restrict carrier mobility, leading to the formation of localized electric fields within the material matrix. Concurrently, charge displacement produces dipole fields oriented in opposition to the external magnetic field, inducing directional polarization throughout the material. When an external electric field is applied, structural defects arising from accumulated stacking dislocations act as polarization centers. These centers undergo relaxation processes, thereby contributing to additional mechanisms of electromagnetic wave attenuation[36, 37].

The Raman spectra of SCNF-1400 to SCNF-1600 are presented in Fig. 1c. It reveals that all five materials exhibit prominent carbon-associated spectral features: a peak at 1342 cm^{-1} attributed to structural irregularities in elemental carbon (D-band), and another at 1578 cm^{-1} corresponding to planar elongation vibrations of sp^2-hybridized carbon atomic networks (G-band). The comparative magnitude ratio between these D and G bands (ID/IG) serves as a quantitative indicator of structural disorder within the graphitic framework, providing insights into both graphitization degree and defect concentration. The calculated I_D/I_G values are 1.15, 1.18, 1.25, 1.03

View Article Online
DOI: 10.1039/D5QI01376C

and 0.94 for SCNF-1400, SCNF-1450, SCNF-1500, SCNF-1550 and SCNF-1600 respectively. The I_D/I_G values of SCNF-1400 to SCNF-1500 showed a gradual increase, indicating that the defects in SCNF nanofibers increased with the increase in pyrolysis temperature. This is due to the fact that the reaction between C and SiO_2 produces more defects and vacancies in C[38]. The increase in defects causes free electrons to be captured by local defects or vacancies, thereby forming dipole polarization and promoting the loss of electromagnetic waves[39]. At the same time, these captured charges form an asymmetric charge distribution around the defect, which in turn generates local dipole polarization. Under the action of an applied electric field, defects acting as polarization centers can enhance dipole polarization, a polarization behavior that converts electromagnetic energy into thermal energy through a relaxation mechanism, thus promoting the dissipation of electromagnetic waves[40-42]. SCNF-1500 to SCNF-1600 showed a decreasing trend in I_D/I_G values, increasing graphitization and decreasing defects[43]. This is due to the action of high temperatures that promote the rearrangement of defective carbon achieving an increase in graphitization and the transition of free carbon from carbon sp^3 bonds to ordered sp^2 graphite according to the three-stage model reported by Ferrari, AC and Robertson, J[44]. The increase in the graphitization degree of the sample is conducive to the improvement of conductive loss.

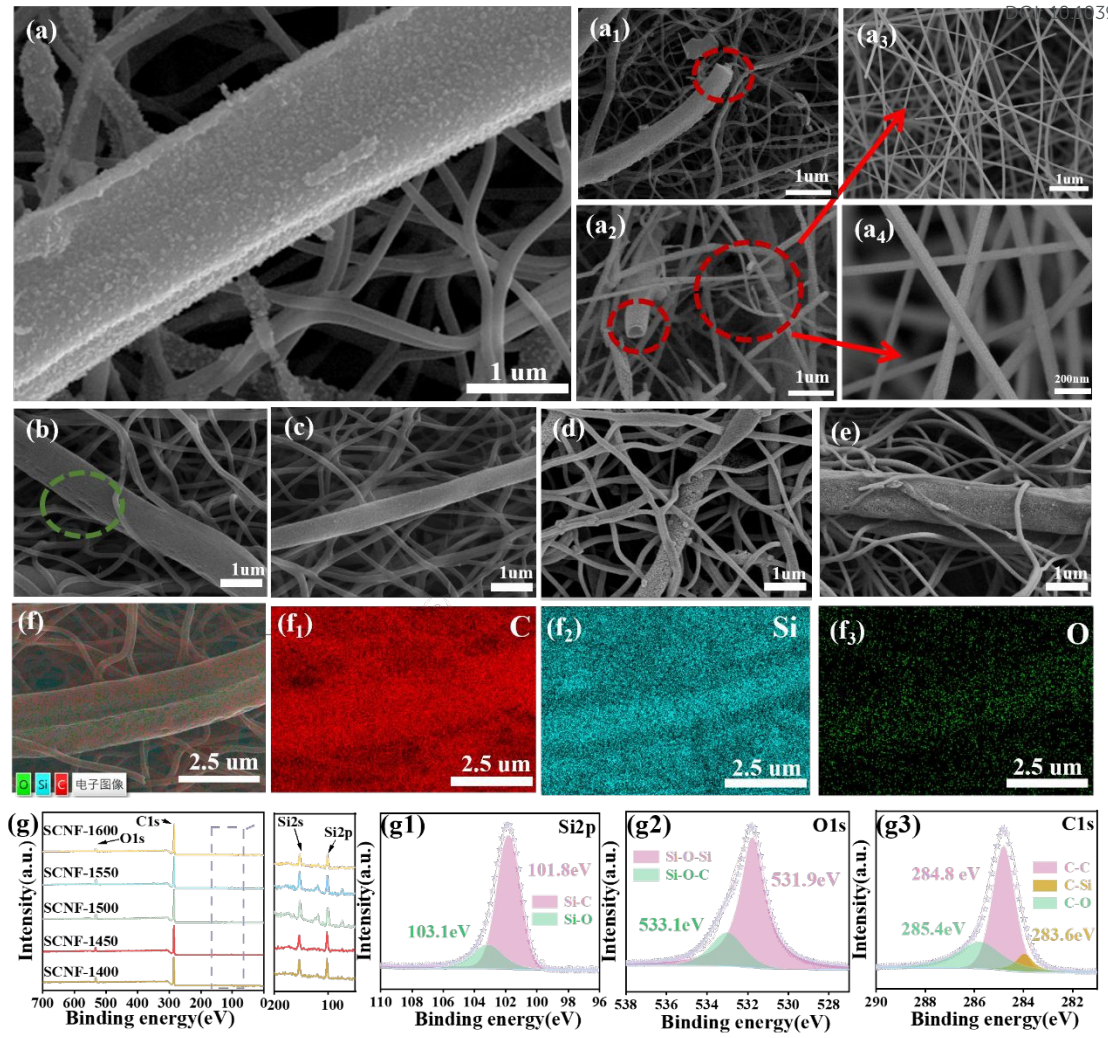

Fig. 2 SEM spectra of SCNF-1450 (a) SCNF-1400 (b) SCNF-1500 (c) SCNF-1550 (d) SCNF-1600 (e); EDS of C, O, and Si of SCNF-1450 (f-f3); XPS spectra of SCNF (g); XPS spectra of SCNF-1450: (g1) Si 2p, (g2) O 1s, (g3) C 1s

The evolution of fiber morphology during carbon thermal reduction was observed by SEM. Fig. 2a-e are SEM images of SCNF-1400, SCNF-1450, SCNF-1500, SCNF-1550, and SCNF-1600, respectively. The SCNF displays a distinctive cobweb-like architecture characterized by the presence of thicker backbone fibers. Moreover, with increasing carbothermal reduction temperature, the surrounding web structure near the coarse fibers becomes progressively denser. At 1450 ℃, the fiber network exhibits enhanced structural integrity, with nanofibers showing improved interconnectivity and continuity. The coarse fibers are identified as SiC@C nanofibers with a core–shell structure, synthesized via electrospinning. The formation of the spider web-like structure is likely attributed to the increased carbothermal reduction temperature, which

View Article Online
DOI: 10.1039/D5QI01376C

promotes the generation of SiO gas through the high-temperature reaction between SiO_2 and carbon within the coarse fibers. As the SiO gas diffuses outward, it undergoes a gas–solid reaction, leading to the growth of a spider web-like SiC network[45]. As shown in Figure 2c-e, the surface roughness of SCNF-1500, SCNF-1550, and SCNF-1600 increases with rising pyrolysis temperature. This can be attributed to the enhanced volatilization of the carbon phase within the nanofibers at higher temperatures. Additionally, worm-like nanowires are observed along the structural edges, likely resulting from SiO gas diffusing through internal pores and reacting with free carbon on the nanofiber surfaces. Figure 2a1-a4 present enlarged SEM images of the localized region of SCNF-1450. As shown in Figure 2a2, the fractured cross-section of the coarse fiber clearly reveals a hollow interior, confirming the presence of a hollow core-shell structure. Figures 2a3 and 2a4 reveals that the gas-solid reaction-derived SiC fibers exhibit numerous entanglement points, forming an interconnected spider web-like architecture. This continuous microstructure promotes efficient electron transport and diffusion pathways, thereby enhancing conductive loss mechanisms and contributing to improved electromagnetic wave attenuation. The EDS information of SCNF-1450 is shown in Figure 2f. It can be observed that SCNF-1450 is composed of C, O, and Si elements, with C and Si evenly distributed throughout the structure, while O is mainly concentrated in the main fibers. This suggests that these main fibers form a hollow SiC structure, while the surrounding spider-web-like fibers are SiC fibers generated through a gas-solid reaction mechanism.

The surface chemistry and bonding state of SCNF nanofibers were studied by XPS. The XPS patterns of SCNF-1400 to SCNF-1600 were displayed in Figure 2g. It reveals four distinct absorption features at binding energies of 532.07, 284.08, 152.07, and 101.07 eV, which correspond to O1s, C1s, Si2s, and Si2p, respectively. These characteristic signals confirm that all SCNF nanofibers are primarily composed of oxygen, carbon, and silicon elements. Two binding peaks, 103.1 and 101.8 eV, are present in the Si2p spectrum of SCNF-1450 (Figure 2g1), which belong to SiO_2 and SiC[36]. In the O1s spectrum (Figure 2g2), the two characteristic peaks of 533.1 eV and 531.9 eV correspond to Si-O-C and Si-O-Si, respectively[46]. The Si-O-C bond may be

related to the SiO_xC_y phase formed by excess silicon atoms, and the Si-O-Si peak is related to SiO_2[47]. These indicates that there are SiC and SiO_2 in SCNF nanofibers. Furthermore, the deconvoluted high-resolution C1s spectral profile (Figure 2g3) exhibits three distinctive energy signatures at 285.4, 284.8, and 283.6 eV, which can be assigned to C-O, C-C, and C-Si bonding configurations, respectively[48]. The C-O signal originates from the attachment of poorly conducting hydroxyl moieties to carbon atoms, while the C-C peak corresponds to elemental carbon generated during high-temperature thermal decomposition processes. The C-Si spectral feature is indicative of silicon carbide formation. Notably, the C-O polar functional groups serve as electrical dipoles, facilitating dipolar polarization mechanisms when subjected to electromagnetic field stimulation. These spectral features collectively confirm the multiphase composition of the sample, including silicon carbide, amorphous silicon dioxide, silicon oxycarbide species, and free carbon.

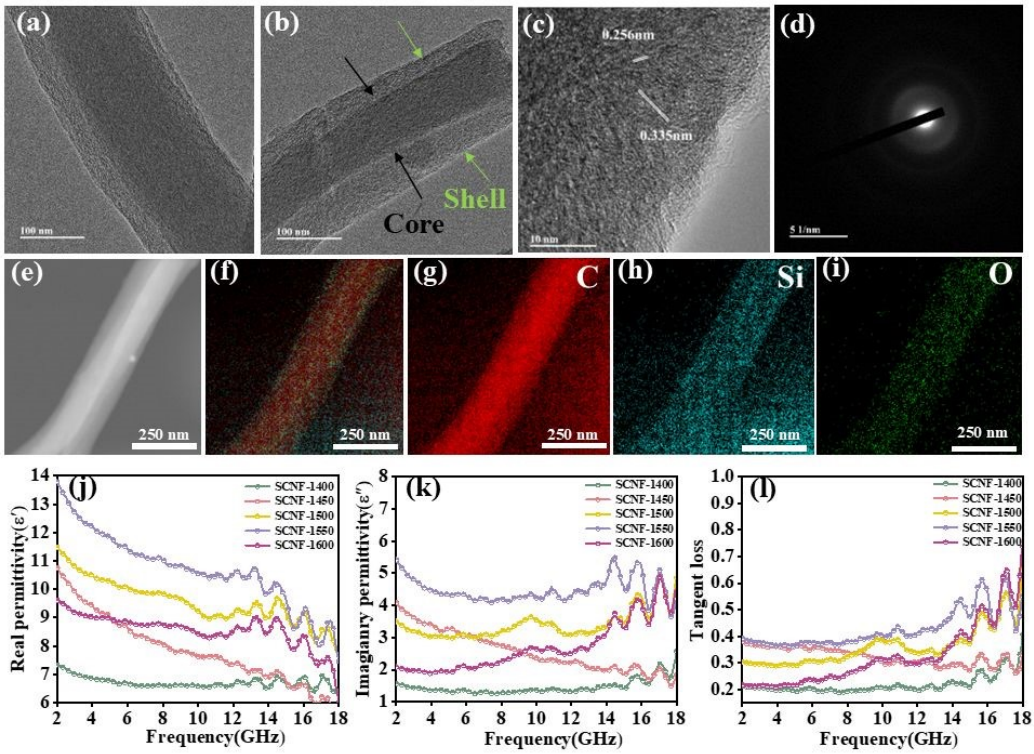

Fig. 3 TEM images (a, b), HRTEM image (c), electron diffraction (d), and elemental distribution maps (e-i) for SCNF-1450; ε′ maps (j), ε″ maps (k), and tanδε maps (l) for SCNF-1400 to SCNF-1600

In order to further analyze the microstructure of SCNF, TEM analysis was

View Article Online
DOI: 10.1039/D5QI01376C

performed on SCNF-1450 (Figures 3a and b). As shown in Fig. 3a and b, SCNF-1450 exhibits a well-defined core-shell nanofiber structure with a relatively uniform fiber diameter. The core layer measures approximately 66.14 nm in diameter, further confirming the successful fabrication of the core–shell architecture. The SCNF-1450 sample exhibits two distinct interplanar spacings: 0.256 nm, corresponding to the (110) plane of silicon carbide, and 0.335 nm, associated with the (002) plane of silicon dioxide. This confirms successful silicon carbide synthesis, while the silicon dioxide crystalline regions represent residual byproducts resulting from polycarbosilane thermal decomposition reactions. Electron diffraction reveals that the edges of the core–shell nanofibers are in an amorphous state, indicating that SCNF-1450 comprises a hollow structure with a SiC shell layer, partially crystalline SiO_2, and partially amorphous SiO_2. This polycrystalline, multiphase architecture creates abundant heterogeneous interfaces, effectively enhancing interfacial polarization and thereby improving electromagnetic wave attenuation[49, 50]. EDS analysis of SCNF-1450, shown in Fig. 3(e-i), reveals a uniform distribution of C, Si, and O throughout the fibers, further indicating the formation of a homogeneous heterogeneous interface.

3.2 EMW absorption performance and mechanism

Electromagnetic parameters determine the wave-absorbing properties of SCNF composites. For the SCNF composites, the primary components are SiC, SiO_2, and carbon, indicating that the material behaves as a dielectric system. Therefore, the influence of complex permeability on the electromagnetic wave absorption properties is not considered. The real (ε′) and imaginary (ε″) parts of the permittivity for SCNF-1400, SCNF-1450, SCNF-1500, SCNF-1550, and SCNF-1600 are presented in Fig. 3j and k. Specifically, the ε′ values for SCNF-1400, SCNF-1450, SCNF-1500, SCNF-1550, and SCNF-1600 range from 7.33–6.34, 10.76–5.54, 11.49–7.48, 13.79–7.45, and 9.61–6.01, respectively. The corresponding ε″ values vary from 1.57–2.58, 4.08–1.84, 3.50–4.85, 5.41–4.10, and 2.08–4.43. Both ε′ and ε″ exhibit a decreasing trend with increasing frequency, which is attributed to the dielectric dispersion phenomenon. According to dispersion theory, dipole reorientation requires a finite response time. At

higher frequencies, dipoles are less able to reorient in phase with the rapidly alternating external electromagnetic field, leading to reduced polarization and a gradual decline in both ε′ and ε″ values[51]. Significant variations in ε′ magnitudes become apparent among the SCNF-1450, SCNF-1500, and SCNF-1550 specimens. These differences are closely linked to temperature-dependent reactions between silicon dioxide and carbon, which initiate the formation of silicon carbide at approximately 1450 °C and approach completion near 1550 °C. The distinct dielectric behaviors stem from the complex multiphase microstructure of these composites, comprising SiO_2, SiC, structurally disordered silicon oxycarbide regions, and amorphous phases. This heterogeneous architecture generates numerous interfacial regions that act as capacitive elements, enhancing electromagnetic energy storage and thereby increasing the ε′ values. Moreover, the abundance of interfacial heterogeneities promotes interfacial polarization, contributing to elevated ε″ values in all three samples. In contrast, the SCNF-1600, subjected to higher thermal reduction, exhibits improved crystallinity and reduced defect density, which in turn leads to a lower ε″ value. The dielectric loss characteristics of SCNF composites are further evaluated using the dielectric loss tangent ($\tan\delta_e = \varepsilon''/\varepsilon'$). Both $\tan\delta_e$ and ε″ display similar trends: relatively stable performance in the 2–13 GHz frequency range, with more pronounced fluctuations between 13 and 18 GHz. Among the samples, SCNF-1450 demonstrates superior dielectric loss performance in the low-to-mid frequency bands, while SCNF-1400, SCNF-1500, SCNF-1550, and SCNF-1600 exhibit enhanced dielectric loss at higher frequencies. This distribution indicates that SCNF-1450 offers particularly effective electromagnetic wave absorption in the lower-frequency region.

In order to quantitatively evaluate the electromagnetic wave attenuation characteristics of SCNF composites, the Cole-Cole semicircle can be used to evaluate its Debye relaxation mechanism in Fig. S(1-5). Cole-Cole semicircle can deeply analyze the conductive dissipation and polarization loss phenomena. The Cole–Cole curves of SCNF-1400 to SCNF-1600 display multiple semicircles with varying radii across the frequency range, indicating the presence of multiple polarization relaxation processes in response to the applied electromagnetic field. SCNF-1450 exhibits a

View Article Online
DOI: 10.1039/D5QI01376C

greater number of semicircles in its Cole-Cole curve, indicating more pronounced polarization relaxation losses. Additionally, the extended straight-line tail observed for SCNF-1450 suggests enhanced conductive loss behavior. In contrast, the Cole-Cole curves of SCNF-1400, SCNF-1500, SCNF-1550, and SCNF-1600 primarily display several distinct semicircles accompanied by shorter linear segments, implying that polarization relaxation is the dominant loss mechanism in these samples. This is because the defects can act as dipole polarization centers, generating dipole rotation polarization under the action of electromagnetic fields, increasing polarization losses. The tail slopes of the Cole-Cole curves for SCNF-1400 to SCNF-1600 are 0.52, 0.48, 0.43, 0.55, and 0.30, respectively, indicating that SCNF-1450 has high conduction losses.

View Article Online
DOI: 10.1039/D5QI01376C

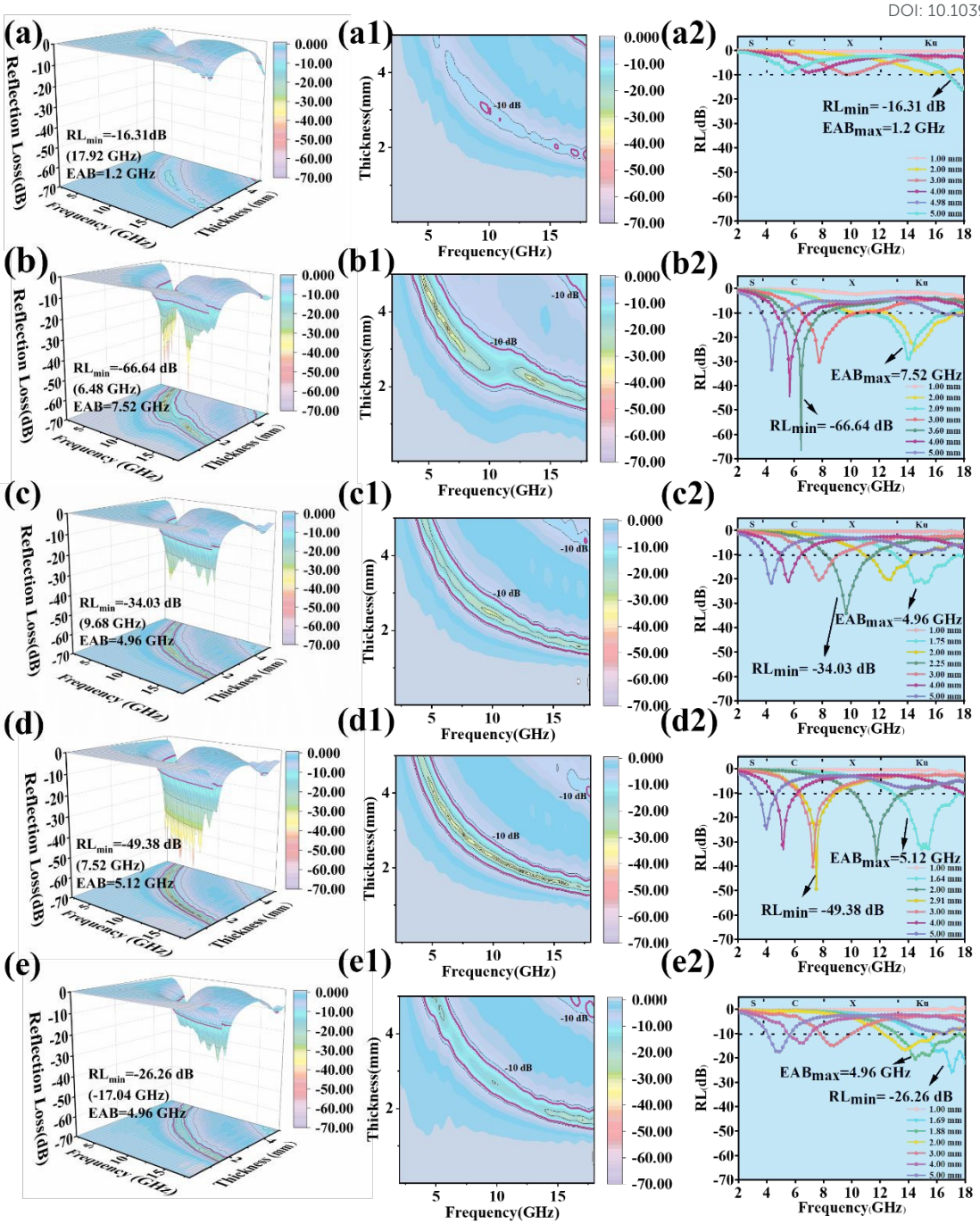

Fig. 4 Three-dimensional, two-dimensional and one-dimensional images of microwave absorption properties of SCNF-1400 (a,a1,a2), SCNF-1450 (b,b1,b2), SCNF-1500 (c,c1,c2), SCNF-1550 (d,d1,d2) and SCNF-1600 (e,e1,e2)

Based on the transmission line theory, the RL value is the key index for evaluating the ability of SCNF composites to EMWs absorb. Figure 4 shows the 3D, 2D and 1D images of the RL curves of SCNF-1400, SCNF-1450, SCNF-1500, SCNF-1550 and SCNF-1600. The RL_{min} values of SCNF-1400, SCNF-1450, SCNF-1500, SCNF-1550,

View Article Online
DOI: 10.1039/D5QI01376C

and SCNF-1600 were -16.31, -66.64, -34.03, -49.38, and -26.26 dB, respectively. The poorest performance observed in SCNF-1400 is attributed to its relatively low pyrolysis temperature. As confirmed by XRD analysis, the limited formation of SiC hinders the development of a well-defined multiphase composite system, thereby resulting in a reduced RL_{min} and narrower EAB_{max}. SCNF-1450, SCNF-1500, and SCNF-1550 have better EMW absorption performance, which is attributed to the fact that all three samples form a polycrystalline multiphase structure providing abundant heterogeneous interfaces. SCNF-1450 exhibits outstanding electromagnetic wave attenuation performance, achieving a minimum reflection loss of -66.64 dB at 6.48 GHz with an optimal thickness of 3.60 mm. Furthermore, when the thickness is 2.09 mm, the composite fiber has a maximum effective absorption bandwidth of 7.52 GHz, covering a frequency range of 9.28 to 16.8 GHz. This excellent electromagnetic wave absorption capability can be attributed to the increased silicon carbide phase content and abundant heterogeneous interfaces in SCNF-1450, which enhance the interfacial polarization process. At the same time, structural defects within the SiC lattice serve as trapping sites for charge carriers, thereby enhancing dipole polarization and promoting additional electromagnetic energy dissipation. In order to better verify the effect of the absorbing material on its stealth, the RCS simulation is used to analyze the signal attenuation after coating (Fig. S6). Figure 5 (d-h) shows the 3D radar scattering signals of SCNF-1400 to SCNF-1600 covered on the PEC conductive layer. It can be seen that the scattering signal of SCNF-1450 is the smallest, which means that the reflected signal is weak and most of the electromagnetic waves are lost after entering the coating. Figure 5 (i) is the 2D curve of RCS after coating the absorbing material. It can be seen that the RCS values of SCNF are lower than the PEC conductive layer between -60° and 60°. It can be seen that the decrease of SCNF-1450 between -20° and 20° is significantly higher than that of other samples, reducing by 40.41 dB m^2, which shows that SCNF-1450 has obvious stealth performance. The simulation results of RCS are consistent with the previous absorbing performance results.

View Article Online
DOI: 10.1039/D5QI01376C

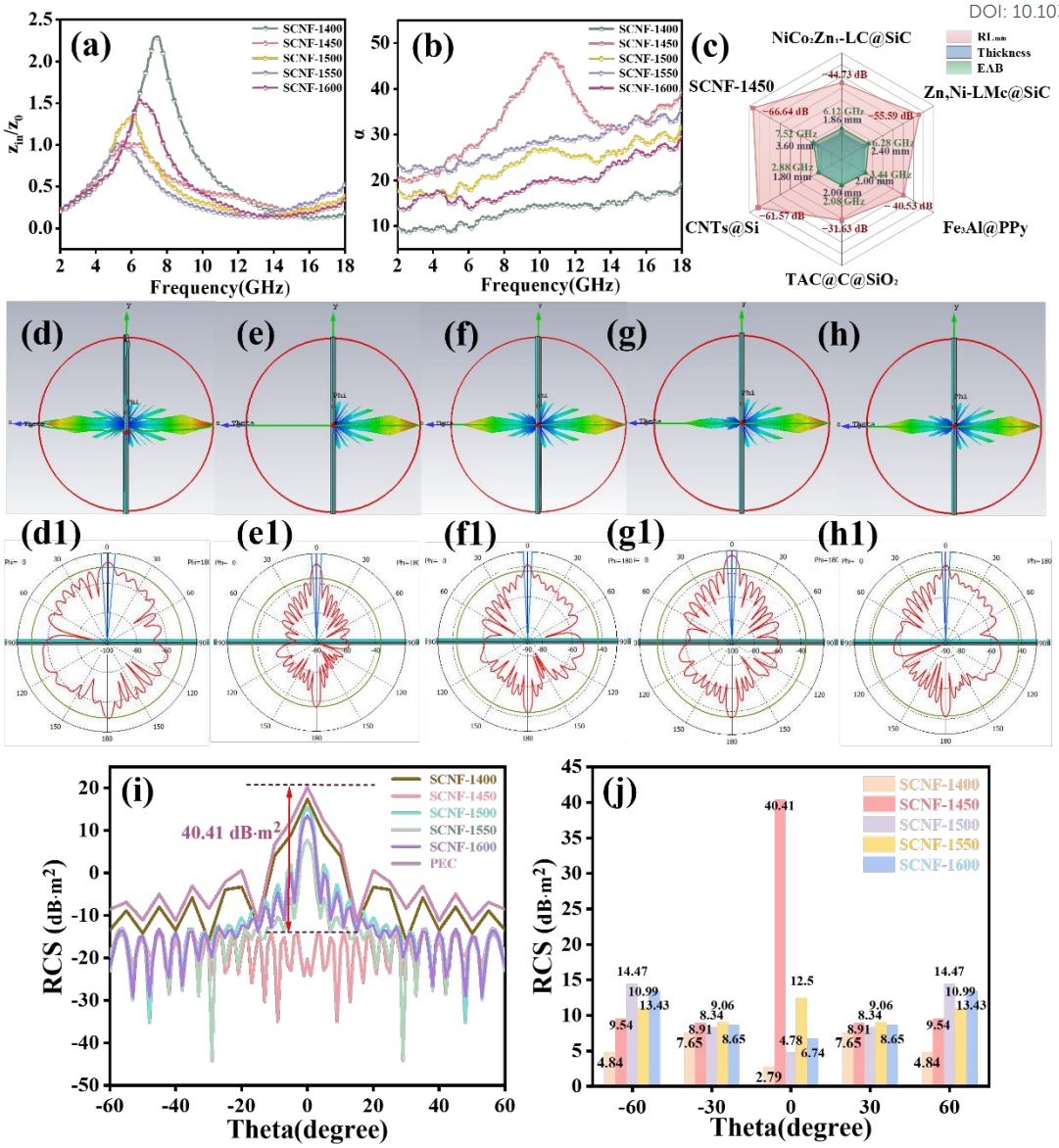

Fig. 5 Impedance matching curve (a) and attenuation constant α (b) for SCNF at 3.6 mm; comparison of SCNF-1450 with excellent core-shell EMW materials (c); CST simulation results (d-h) and RSC values of-180° ~ 180° (d1-h1) for SCNF-1400 to SCNF-1600, RCS values at different detection angles (i and j)

It is well known that the characteristics of impedance matching are critical for electromagnetic wave absorption performance. When the output impedance of an electromagnetic wave absorbing material closely matches that of free space, it enables greater penetration of electromagnetic waves into the interior of the absorber[52, 53]. In other words, the material exhibits good impedance matching when the ratio of input impedance to free space impedance (Z_{in}/Z_0) falls within the range of 0.8 to 1.2[54]. Figure 5a shows the impedance matching curve of SCNF composite at 3.60 mm. SCNF-

1450 exhibits optimal impedance matching across the entire frequency range. In the 4.44-7.44 GHz (3.0 GHz) frequency band, its Z value is in the range of 0.8-1.2, demonstrating excellent impedance matching. In contrast, SCNF-1400, SCNF-1500, SCNF-1550, and SCNF-1600 satisfy the above intervals only in the range of 1.84 GHz, 1.68 GHz, 2.16 GHz, and 1.60 GHz, respectively. α is an indicator for evaluating the electromagnetic wave attenuation efficiency of an absorbing material. The higher the α value, the stronger the attenuation capability. SCNF-1400, SCNF-1500, SCNF-1550, and SCNF-1600 display monotonically increasing attenuation constants with frequency progression in Figure 5b. The changes of SCNF-1450 were more complex, first increasing, then decreasing, and finally increasing across the entire spectrum. Notably, SCNF-1450 exhibits significantly higher attenuation constants than the other samples across the entire measured frequency range, with a particularly prominent peak of 236.46 in the mid-frequency region. This remarkable value highlights the superior electromagnetic wave attenuation capability of the SCNF-1450.

Table 1: Comparison of the EMW absorption performance of SCNF-1450 with excellent core-shell structural wave absorbing materials in recent years

Samples	RL_{min}(dB)	Thickness(mm)	EAB(GHz)	References
$NiCo_2Zn_1$-LC@SiC	−44.73 dB	1.86 mm	6.12 GHz	[55]
Zn,Ni-LMc@SiC	−55.59 dB	2.40 mm	6.28 GHz	[56]
Fe_3Al@PPy	− 40.53 dB	2.00 mm	3.44 GHz	[57]
TAC@C@SiO_2	−31.63 dB	2.00 mm	2.08 GHz	[58]
CNTs@Si	−61.57 dB	1.80 mm	2.88 GHz	[59]
SCNF-1450	−66.64 dB	3.60 mm	7.52 GHz	This work

A comparative analysis of recently reported core-shell structured electromagnetic wave absorbers highlights the superior attenuation performance of SCNF-1450, as depicted in Figure 5c and detailed in Table 1. The SCNF-1450 composite distinctly meets several key criteria for high-performance electromagnetic wave absorbers, including minimal matching thickness, low density, broad effective absorption bandwidth, and strong attenuation capability. These attributes underscore its potential as a highly promising candidate for advanced wave absorption applications. The observed enhancement in performance is consistent with the previously discussed dielectric loss mechanisms.

View Article Online
DOI: 10.1039/D5QI01376C

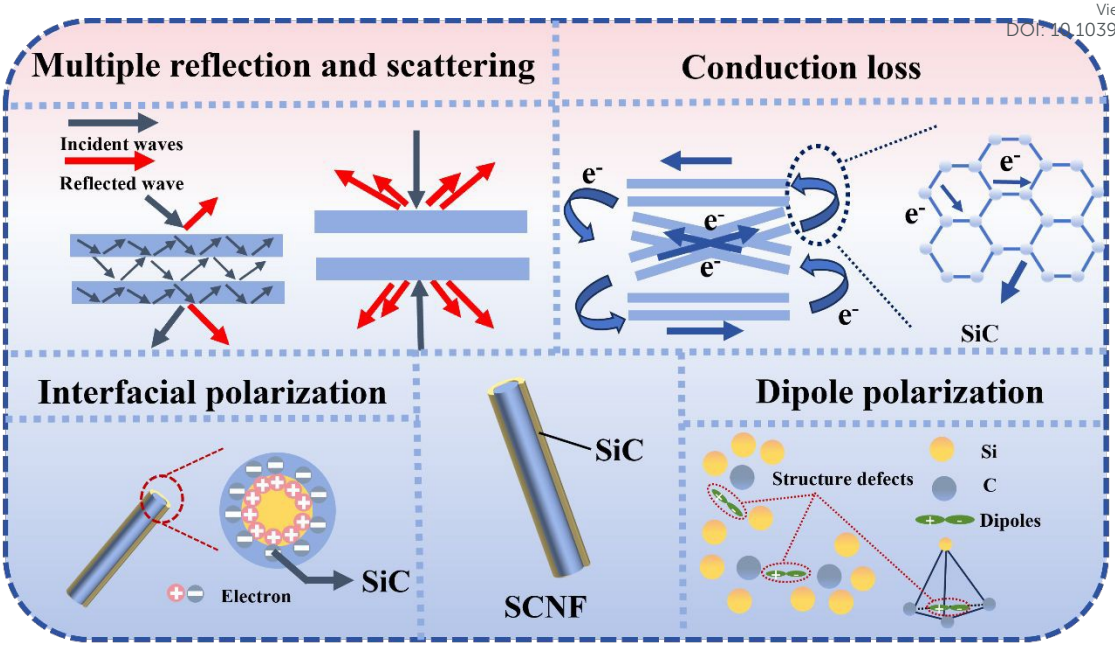

Fig. 6 Schematic diagram of SCNF-1450 microwave absorption mechanism

Figure 6 offers further insight into EMW absorption behavior of SCNF composites from the perspective of dielectric dissipation. The unique architecture of SCNF-1450 features internal voids that introduce a gaseous phase into composites matrix, effectively tuning its dielectric properties. Additionally, the presence of amorphous silicon dioxide acts as a wave-transparent phase with a relatively low dielectric constant, contributing to the optimization of overall dielectric performance. Together, these structural and compositional features significantly enhance impedance matching, allowing a greater proportion of incident EMW to penetrate the absorber-a prerequisite for efficient attenuation. Secondly, the gas-solid composite structure of SCNF-1450 promotes the formation of a spider web-like SiC network. This web structure offers extensive pathways for electron transport. Furthermore, the residual graphitic carbon present on the coarse SiC fibers provides additional conductive channels, facilitating the dissipation of EMW energy through conduction losses.Thirdly, the coexistence of a hollow core, SiC shell, amorphous SiO_2, and SiO_xC_y phases generates numerous heterogeneous interfaces within the SCNF structure. These interfaces give rise to strong interfacial polarization effects, which further consume EMW energy[60]. Finally, the high density of structural defects (e.g., stacking faults or layer mismatches) in the SiC phase can act as polarization centers that trap charge carriers, induce dipolar polarization, and contribute additional energy loss[61]. In summary, the exceptional EMW attenuation capabilities of SCNFs can be attributed to the synergistic effects of multiple mechanisms, including conductive loss, interfacial polarization, dipolar polarization, and the unique hollow spider web-like architecture.

View Article Online
DOI: 10.1039/D5QI01376C

4 Conclusion

In summary, spider-web-like core-shell SiC@C nanofibers (SCNFs) were successfully fabricated via coaxial electrospinning followed by high-temperature pyrolysis. The SCNFs exhibited distinct EMW absorption characteristics. Notably, SCNF-1450 achieved RL_{min} of –66.64 dB at an optimal thickness of 3.60 mm, and EAB_{max} of 7.52 GHz at a thickness of 2.09 mm. The unique spider web-like architecture, consisting of primary SiC fibers with internal voids, promotes the formation of an interconnected conductive network that enhances conductive loss mechanisms. Simultaneously, the hierarchical structure-including hollow cores, SiC shells, and amorphous SiO_2 and SiO_xC_y phases-introduces a high density of heterogeneous interfaces. These interfaces, together with abundant crystallographic defects such as stacking faults in the SiC lattice, intensify interfacial and dipolar polarization effects, contributing significantly to EMW attenuation.This study provides valuable insights into the design of high-temperature-resistant, SiC-based materials with enhanced EMW absorption performance.

Acknowledgement

This work was financially supported by the National Natural Science Foundation of China (Grant No.52102036), and the Sichuan Science and Technology Program (2021JDRC0099).

References

[1] HAN Y, GUO H, QIU H ,et al. Multimechanism Decoupling for Low-Frequency Microwave Absorption Hierarchical Fe-Doped Co Magnetic Microchains [J]. Advanced Functional Materials, 2025, 10.1002/adfm.202506803.

[2] HE M, ZHONG X, LU X ,et al. Excellent Low-Frequency Microwave Absorption and High Thermal Conductivity in Polydimethylsiloxane Composites Endowed by Hydrangea-Like CoNi@BN Heterostructure Fillers [J]. Advanced Materials, 2024, 36(48), 2410186.

[3] ZHOU L, HU P, BAI M ,et al. Harnessing the Electronic Spin States of Single Atoms for Precise Electromagnetic Modulation [J]. Advanced Materials, 2025, 37(7), 2418321.

[4] ZHANG S, ZHENG J, LAN D ,et al. Hierarchical Engineering on Built-In Electric

Field of Bimetallic Zeolitic Imidazolate Derivatives Towards Amplified Dielectric Loss [J]. Advanced Functional Materials, 2025, 35(3), 2413884.

[5] ZHANG S, ZHENG J, ZHAO Z ,et al. New Prospects in Built-In Electric Fields for Electromagnetic Wave Absorption: from Fundamentals to Interdisciplinary Applications [J]. Advanced Functional Materials, 2025, e13762.

[6] ZHONG X, HE M, ZHANG C ,et al. Heterostructured BN@Co-C@C Endowing Polyester Composites Excellent Thermal Conductivity and Microwave Absorption at C Band [J]. Advanced Functional Materials, 2024, 34(19), 2313544.

[7] QIAN J, DU B, CAI M ,et al. Preparation of SiC Nanowire/Carbon Fiber Composites with Enhanced Electromagnetic Wave Absorption Performance [J]. Advanced Engineering Materials, 2021, 23(10), 2100434.

[8] TANG L, JIANG J, HE M ,et al. Lightweight PBO nanofiber@ZIF-67 derived carbon aerogel with superior electromagnetic wave absorption and thermal insulation [J]. Journal of Materials Science & Technology, 2026, 244, 186-195.

[9] XIAO-XUAN F, XIN-CI Z, LIN L ,et al. Recent progress and perspective of microwave absorption materials derived from metal-organic frameworks [J]. Soft Science, 2024, 4(4), 43.

[10] SHU R, ZHANG G, ZHANG C ,et al. Nitrogen-Doping-Regulated Electromagnetic Wave Absorption Properties of Ultralight Three-Dimensional Porous Reduced Graphene Oxide Aerogels [J]. Advanced Electronic Materials, 2021, 7(2), 2001001.

[11] LV Q, SUN X, ZHANG C ,et al. Porous nickel–zinc ferrite/polyaniline/polyimide composite based on improved impedance matching for electromagnetic microwave absorption [J]. Polymer Composites, 2022, 43(12), 8737-8748.

[12] YANG N, XU S, ZHANG D ,et al. Super-Wideband Electromagnetic Absorbing TiC/SiOC Ceramic/Glass Composites Derived from Polysiloxane and Titanium Isopropoxide with Low Thickness (<1 mm) [J]. Advanced Engineering Materials, 2023, 25(9), 2201508.

[13] ZHANG B, TONG Z, WANG X ,et al. Zirconium-modified hierarchical porous SiC-based nanofibrous aerogel with efficient electromagnetic waves absorption

and thermal insulation properties [J]. Journal of the European Ceramic Society, 2025, 45(1), 116808.

[14] YU S, ZENG T, YANG Y ,et al. Effect of an annealing treatment on the microstructure and EMW-absorbing properties of SiCw/Si_3N_4 ceramics fabricated by 3D printing [J]. Ceramics International, 2023, 49(1), 1092-1101.

[15] WU Y, ZHONG Y, GUAN Y ,et al. Polymer-derived Co_2Si@SiC/C/SiOC/SiO_2/Co_3O_4 nanoparticles: Microstructural evolution and enhanced EM absorbing properties [J]. Journal of the American Ceramic Society, 2020, 103(12), 6764-6779.

[16] XIANG D, HE Q, FAN C ,et al. Preparation and 3D network structure optimization of SiC and SiC@Fe_3Si nanofibers for enhanced electromagnetic wave absorption [J]. Materials Today Nano, 2025, 30, 100644.

[17] XU Z, LI F, WANG Y ,et al. Microstructure and oxidation resistance of ZrB_2–ZrC–SiC composite nanofibers fabricated via electrospinning combined with carbothermal reduction [J]. Ceramics International, 2021, 47(14), 20740-20744.

[18] WU D, DENG S, WANG Y ,et al. Hierarchical porous carbon fibers for broadband and tunable high-performance microwave absorption [J]. Materials Research Bulletin, 2024, 172, 112653.

[19] WANG Y, XIAO P, ZHOU W ,et al. Microstructures, dielectric response and microwave absorption properties of polycarbosilane derived SiC powders [J]. Ceramics International, 2018, 44(4), 3606-3613.

[20] YAN M, CHENG X, GONG L ,et al. Growth mechanism and structure regulation of super-elastic SiC aerogels for thermal insulation and electromagnetic wave absorption [J]. Chemical Engineering Journal, 2023, 475, 146417.

[21] LIU D, ZHOU Z, WANG Y ,et al. Preparation and characterization of polymer-derived SiC ceramic aerogels toward excellent electromagnetic wave absorption properties [J]. Journal of Materials Research and Technology, 2022, 19, 507-519.

[22] ZHAO H, LIU W, LIU J ,et al. Size-dependent electromagnetic wave absorption of 3C–SiC particles [J]. Journal of Materials Chemistry C, 2024, 12(35), 14054-14061.

[23] WANG Y, YUAN X, PING Z ,et al. Structure engineering by Zn sublimation to enhance electromagnetic wave absorption performance of SiC/C nanofibers [J]. Ceramics International, 2025, 51(17), 24327-24333.

[24] WANG Y, WANG C, CHEN Z ,et al. Electroless plated of Ni-P@SiC nanowire composite for high-performance EMW absorption by tailoring impedance matching [J]. Journal of Alloys and Compounds, 2025, 1014, 178795.

[25] ZHANG Y, ZHANG L, SI H ,et al. TiN nanofiber metacomposites for efficient electromagnetic wave absorption: Insights on multiple reflections and scattering effects [J]. Journal of Materials Science & Technology, 2025, 233, 69-79.

[26] XU B, HE Q, WANG Y ,et al. Novel accordion-like structure of SiC/C composites for enhanced electromagnetic wave absorption [J]. Carbon, 2023, 215, 118470.

[27] QIAN J, WANG T, SHAN Q ,et al. Design of porous SiC/MnO_2 bulk composite with improved absorption of low-frequency electromagnetic waves [J]. Journal of Alloys and Compounds, 2024, 978, 173359.

[28] YANG D, DONG S, CUI T ,et al. Lightweight and robust electrospun zirconia fiber reinforced carbon aerogel composites for efficient microwave absorption and heat insulation [J]. Carbon, 2024, 228, 119387.

[29] ZHANG B, WEN X, MA C. Nitrogen-doped bean-like SiC-based nanofibers for thermal insulation and electromagnetic wave absorption [J]. Journal of Alloys and Compounds, 2024, 1001, 175173.

[30] ZHANG M, CHANG M, TIAN W ,et al. Interfacial modulation of SiC/TiC hybrid nanofibers for fabricating flexible ceramic electromagnetic wave absorbers [J]. Materials Research Bulletin, 2024, 178, 112883.

[31] LIN D, PENG J, GUO J ,et al. Unique frequency reversible conversion and bandwidth regulation of electromagnetic wave absorption performance for core-shell structured Fe_3O_4 and manganese oxide composites [J]. Materials Today Nano, 2025, 29, 100568.

[32] CHEN N, CHEN T, DING J ,et al. Study on the microwave absorbing properties of SiC@Ni powders with core@shell structure [J]. Next Materials, 2024, 5, 100242.

[33] WANG P, LI Z, CHENG L ,et al. SiC/rGO Core–Shell Nanowire as a Lightweight, Highly Efficient Gigahertz Electromagnetic Wave Absorber [J]. ACS Applied Electronic Materials, 2020, 2(2), 473-482.

[34] OWOEYE S S, ABEGUNDE S M, OJI B. Effects of process variable on synthesis and characterization of amorphous silica nanoparticles using sodium silicate solutions as precursor by sol–gel method [J]. Nano-Structures & Nano-Objects, 2021, 25, 100625.

[35] CHEN J, SHI Q, TANG W. Field emission performance of SiC nanowires directly grown on graphite substrate [J]. Materials Chemistry and Physics, 2011, 126(3), 655-659.

[36] XIANG Z, HE Q, WANG Y ,et al. Preparation and electromagnetic wave absorption properties of SiC/SiO_2 nanocomposites with different special structures [J]. Applied Surface Science, 2022, 599, 153968.

[37] XU B, HE Q, WANG Y ,et al. Construction of magnetic nanoparticle channels in SiC/SiO_2 composite foam toward efficient electromagnetic wave absorption [J]. Applied Surface Science, 2023, 636, 157839.

[38] TAN F, GUO H, WANG Z ,et al. Electrospinning-enabled SiO_x@TiO_2/C fibers as anode materials for lithium-ion batteries [J]. Journal of Alloys and Compounds, 2021, 888, 161635.

[39] ZHOU X, ZHANG W, ZHAO Z ,et al. The luminescence enhancement of $NaLaSiO_4$:Tb^{3+} green phosphor by co-substituting Si^{4+}-O^{2-}/La^{3+}-O^{2-} with B^{3+}-F^-/Ba^{2+}-F^- for white light-emitting diodes [J]. Ceramics International, 2025, 51(10), 12831-12841.

[40] ZHANG K, YAN Y, WANG Z ,et al. Integration of Electrical Properties and Polarization Loss Modulation on Atomic Fe–N-RGO for Boosting Electromagnetic Wave Absorption [J]. Nano-Micro Letters, 2024, 17(1), 46.

[41] ZHANG H, WANG B, FENG A ,et al. Mesoporous carbon hollow microspheres with tunable pore size and shell thickness as efficient electromagnetic wave absorbers [J]. Composites Part B: Engineering, 2019, 167, 690-699.

[42] ZHANG S, ZHENG J, LV C ,et al. Synergistic enhancement of defect-induced

polarization and built-in electric field effect in carbon hybrids towards efficient electromagnetic wave absorption [J]. Carbon, 2025, 234, 120037.

[43] WANG B, LI C, NI C ,et al. Facile synthesis of heterogeneous Co/MnO@C nanocapsules with dual-cores: Achieving strong and broadband microwave absorption by magnetic-dielectric synergy [J]. Applied Surface Science, 2023, 614, 156228.

[44] WANG W, NAN K, ZHENG H ,et al. Heterostructure design of one-dimensional ZnO@CoNi/C multilayered nanorods for high-efficiency microwave absorption [J]. Journal of Colloid and Interface Science, 2024, 657, 491-501.

[45] SU J, GAO B, CHEN Z ,et al. Large-Scale Synthesis and Mechanism of β-SiC Nanoparticles from Rice Husks by Low-Temperature Magnesiothermic Reduction [J]. ACS Sustainable Chemistry & Engineering, 2016, 4(12), 6600-6607.

[46] ZANG J, LI H, ZHU Q ,et al. High efficiency microwave absorption properties of α−SiCp/ α −SiCnw/SiO_2/C composites with multi−interface hybrid SiC nanowires prepared by heterogeneous nucleation−growth mechanism [J]. Journal of Alloys and Compounds, 2025, 1014, 178759.

[47] XIANG Z, WANG Y, YIN X ,et al. Microwave absorption performance of porous heterogeneous SiC/SiO_2 microspheres [J]. Chemical Engineering Journal, 2023, 451, 138742.

[48] XIANG Z, HE Q, WANG Y ,et al. Hollow porous SiC spheres prepared by in-situ reaction with efficient microwave absorption [J]. Ceramics International, 2022, 48(23, Part A), 35317-35327.

[49] ZHANG Q, LAN D, DENG S ,et al. Constructing multiple heterogeneous interfaces in one-dimensional carbon fiber materials for superior electromagnetic wave absorption [J]. Carbon, 2024, 226, 119233.

[50] ZHANMING W, JUN H, XIAOJUN Z. Dual magnetic particles modified carbon nanosheets in CoFe/Co@NC heterostructure for efficient electromagnetic synergy [J]. Soft Science, 2024, 4(4), 42.

[51] LIANG C, WANG Z. Eggplant-derived SiC aerogels with high-performance electromagnetic wave absorption and thermal insulation properties [J]. Chemical

View Article Online
DOI: 10.1039/D5QI01376C

Engineering Journal, 2019, 373, 598-605.

[52] YAO L, WANG Y, ZHAO J ,et al. Multifunctional Nanocrystalline-Assembled Porous Hierarchical Material and Device for Integrating Microwave Absorption, Electromagnetic Interference Shielding, and Energy Storage [J]. Small, 2023, 19(25), 2208101.

[53] FENG Y, ZHANG L, LI Z ,et al. Ultralight reduced graphene oxide/SiO_2–C nanofibers composite aerogel decorated with $Li_{0.35}Zn_{0.3}Fe_{2.35}O_4$ nanoparticles with a three-dimensional bridging network for efficient electromagnetic wave absorption [J]. Carbon, 2023, 215, 118435.

[54] QIN M, ZHANG L, ZHAO X ,et al. Lightweight Ni Foam-Based Ultra-Broadband Electromagnetic Wave Absorber [J]. Advanced Functional Materials, 2021, 31(30), 2103436.

[55] XU Z, ZHANG K, LI Y ,et al. Synthesis of SiC nanowires wrapped in trimetallic layered double hydroxide nanosheets with core-shell structure via self-assembly growth approach for effective electromagnetic wave absorption [J]. Journal of Alloys and Compounds, 2024, 976, 173316.

[56] ZHANG K, XU Z, CHENG S ,et al. Ambient synthesis of one-dimensional core-shell nanocomposites by encapsulating SiC nanowires with layered double hydroxide nanosheets for high-performance microwave absorption application [J]. Materials Today Physics, 2024, 40, 101289.

[57] SHEN Y, SONG P, ZHANG F ,et al. Core-shell Fe_3Al@polypyrrole composites with tunable shell thickness and enhanced microwave absorption performance [J]. Colloids and Surfaces A: Physicochemical and Engineering Aspects, 2024, 682, 132814.

[58] GUO Y, GUO X, JIAN X. High-temperature stability core-shell engineered Ti_3AlC_2@C@SiO_2 for excellent microwave absorbing properties [J]. Vacuum, 2023, 212, 112049.

[59] ZHOU J, WANG X, GE K ,et al. Core-shell structured nanocomposites formed by silicon coated carbon nanotubes with anti-oxidation and electromagnetic wave absorption [J]. Journal of Colloid and Interface Science, 2022, 607, 881-889.

[60] YAO L-H, SHU J-C, ZHAO J-G ,et al. Heterodimensional Structure Integrating Electromagnetic Functions and Hybrid Energy Storage to Drive Multifunctional Devices [J]. Advanced Functional Materials, 2025, 35, 2503307.

[61] SUN X, LI X, CHEN P ,et al. Controllable regulation of defects in nitrogen-doped hollow core-shell magnetoelectric microspheres towards preferable electromagnetic absorption [J]. Carbon, 2025, 234, 119963.

View Article Online
DOI: 10.1039/D5QI01376C

Data availability

Data will be made available on request.